University Library

MINERVA ACCESS

A gateway to Melbourne's research publications

Minerva Access is the Institutional Repository of The University of Melbourne

Author/s:
Luo, Z;Morey, JR;Deplazes, E;Motygullina, A;Tan, A;Ganio, K;Neville, SL;Eleftheriadis, N;Isselstein, M;Pederick, VG;Paton, JC;Cordes, T;Harmer, JR;Kobe, B;McDevitt, CA

Title:
A trap-door mechanism for zinc acquisition by streptococcus pneumoniae adca

Date:
2021-01-01

Citation:
Luo, Z., Morey, J. R., Deplazes, E., Motygullina, A., Tan, A., Ganio, K., Neville, S. L., Eleftheriadis, N., Isselstein, M., Pederick, V. G., Paton, J. C., Cordes, T., Harmer, J. R., Kobe, B. & McDevitt, C. A. (2021). A trap-door mechanism for zinc acquisition by streptococcus pneumoniae adca. Mbio, 12 (1), pp.1-14. https://doi.org/10.1128/mBio.01958-20.

Persistent Link:
https://hdl.handle.net/11343/272818

License:
CC BY

AMERICAN SOCIETY FOR MICROBIOLOGY | mBio®

RESEARCH ARTICLE
Host-Microbe Biology

A Trap-Door Mechanism for Zinc Acquisition by *Streptococcus pneumoniae* AdcA

Zhenyao Luo,[a,b,c] Jacqueline R. Morey,[d] Evelyne Deplazes,[e,f] Alina Motygullina,[g] Aimee Tan,[h] Katherine Ganio,[h] Stephanie L. Neville,[h] Nikolaos Eleftheriadis,[j] Michael Isselstein,[k] Victoria G. Pederick,[d] James C. Paton,[i] Thorben Cordes,[j,k] Jeffrey R. Harmer,[f] Bostjan Kobe,[a,b,c] Christopher A. McDevitt[d,h]

[a]School of Chemistry and Molecular Biosciences, University of Queensland, Brisbane, Queensland, Australia
[b]Australian Infectious Diseases Research Centre, University of Queensland, Brisbane, Queensland, Australia
[c]Institute for Molecular Bioscience, University of Queensland, Brisbane, Queensland, Australia
[d]Department of Molecular and Biomedical Science, School of Biological Sciences, University of Adelaide, Adelaide, South Australia, Australia
[e]School of Life Sciences, University of Technology Sydney, Ultimo, New South Wales, Australia
[f]School of Pharmacy and Biomedical Sciences, Curtin Health Innovation Research Institute, Curtin University, Bentley, Western Australia, Australia
[g]Centre for Advanced Imaging, The University of Queensland, St. Lucia, Queensland, Australia
[h]Department of Microbiology and Immunology, The Peter Doherty Institute for Infection and Immunity, University of Melbourne, Melbourne, Victoria, Australia
[i]Research Centre for Infectious Diseases, Department of Molecular and Biomedical Science, School of Biological Sciences, University of Adelaide, Adelaide, South Australia, Australia
[j]Molecular Microscopy Research Group, Zernike Institute for Advanced Materials, University of Groningen, Groningen, The Netherlands
[k]Physical and Synthetic Biology, Faculty of Biology, Ludwig Maximilians-Universität München, Planegg-Martinsried, Germany

Zhenyao Luo and Jacqueline R. Morey contributed equally to this article. The author order was determined based on relative contributions to the study.

ABSTRACT Zinc is an essential element in all domains of life. Nonetheless, how prokaryotes achieve selective acquisition of zinc from the extracellular environment remains poorly understood. Here, we elucidate a novel mechanism for zinc-binding in AdcA, a solute-binding protein of *Streptococcus pneumoniae*. Crystal structure analyses reveal the two-domain organization of the protein and show that only the N-terminal domain ($AdcA_N$) is necessary for zinc import. Zinc binding induces only minor changes in the global protein conformation of AdcA and stabilizes a highly mobile loop within the $AdcA_N$ domain. This loop region, which is conserved in zinc-specific solute-binding proteins, facilitates closure of the $AdcA_N$ binding site and is crucial for zinc acquisition. Collectively, these findings elucidate the structural and functional basis of selective zinc uptake in prokaryotes.

IMPORTANCE Zinc is an essential nutrient for the virulence of bacterial pathogens such as *Streptococcus pneumoniae*. Many Gram-positive bacteria use a two-domain lipoprotein for zinc acquisition, but how this class of metal-recruiting proteins acquire zinc and interact with the uptake machinery has remained poorly defined. We report the first structure of a two-domain lipoprotein, AdcA from *S. pneumoniae*, and use computational, spectroscopic, and microbiological approaches to provide new insights into the functional basis of zinc recruitment. Our findings reveal that AdcA employs a novel mechanism for zinc binding that we have termed the "trap-door" mechanism, and we show how the static metal-binding site of the protein, which confers its selectivity for zinc ions, is combined with a dynamic surface element to facilitate zinc recruitment and import into the bacterium. Together, these findings expand our understanding of how bacteria acquire zinc from the environment and provide a foundation for inhibiting this process, through antimicrobial targeting of the dynamic structural elements to block bacterial zinc scavenging.

KEYWORDS ABC transporter, solute-binding protein, *Streptococcus pneumoniae*, zinc

Citation Luo Z, Morey JR, Deplazes E, Motygullina A, Tan A, Ganio K, Neville SL, Eleftheriadis N, Isselstein M, Pederick VG, Paton JC, Cordes T, Harmer JR, Kobe B, McDevitt CA. 2021. A trap-door mechanism for zinc acquisition by *Streptococcus pneumoniae* AdcA. mBio 12:e01958-20. https://doi.org/10.1128/mBio.01958-20.

Editor Justin A. Thornton, Mississippi State University

Copyright © 2021 Luo et al. This is an open-access article distributed under the terms of the Creative Commons Attribution 4.0 International license.

Address correspondence to Bostjan Kobe, b.kobe@uq.edu.au, or Christopher A. McDevitt, christopher.mcdevitt@unimelb.edu.au.

Received 14 October 2020
Accepted 11 December 2020
Published 2 February 2021

The d-block metal ion zinc (Zn^{2+}) is essential for all forms of life. In prokaryotes, Zn^{2+} serves as a crucial structural and/or catalytic cofactor in ca. 5 to 6% of the proteome and is involved in critical processes such as carbon metabolism, competence, and the regulation of DNA transcription (1). The essentiality of Zn^{2+} necessitates that pathogenic organisms scavenge this element from the host environment. Despite the relative abundance of Zn^{2+} in vertebrate hosts, its bioavailability is tightly controlled. To overcome host Zn^{2+} restriction, pathogenic bacteria, including *Streptococcus pneumoniae* (2, 3), *Escherichia coli* (4), *Pseudomonas aeruginosa* (5, 6), *Staphylococcus aureus* (7), and *Salmonella enterica* serovar Typhimurium (8), employ high-affinity Zn^{2+} uptake pathways. In animal models of infection, Zn^{2+}-scavenging pathways primarily belong to the type II ATP-binding cassette (ABC) family of importers (9) but can also include the zinc-iron permease transporters (10), P-type ATPases (11), and zincophore scavenging systems (7). Bacterial ABC permeases are comprised of an extracytoplasmic solute-binding protein (SBP), which recruits ligands from the bulk solvent, and an ABC transporter, which facilitates cellular import (9). How Zn^{2+}-specific SBPs achieve metal ion cargo selection from the complex chemical milieu of the host environment has remained unclear.

S. pneumoniae (the pneumococcus) is the leading cause of bacterial pneumonia, which accounts for 15% of all childhood disease mortalities, and has a global economic health burden of more than US$4 billion annually (12, 13). Zinc is essential for virulence and survival and is acquired solely by the ABC transporter, AdcCB, and two Zn^{2+}-specific cluster A-I SBPs, AdcA and AdcAII, in *S. pneumoniae* (3, 14, 15). AdcA and AdcAII have overlapping functional roles with respect to Zn^{2+} recruitment, with either SBP sufficient for *in vitro* Zn^{2+} homeostasis (2, 3). Nevertheless, both SBPs are required for full virulence, indicating that AdcA and AdcAII have complementary roles during infection (3). The presence of two Zn^{2+}-specific SBPs is highly atypical, since most prokaryotes encode only one. However, this arrangement allows AdcA and AdcAII to be differentially regulated in response to Zn^{2+} abundance, thereby enhancing pneumococcal survival *in vivo* (3). AdcA and AdcAII, which share 43% sequence identity over 265 amino acids, belong to the cluster A-I subgroup of SBPs and have a conserved structural fold, comprising a two-lobed organization with N- and C-terminal $(\beta/\alpha)_4$ domains, connected by a rigid lobe-linking α-helix (16–18). The metal-binding site is located within the cleft that bisects the protein surface. Although both SBPs share this structural core, AdcA also has a C-terminal domain (residues 322 to 501; here termed $AdcA_C$) that is structurally related to ZinT, a periplasmic protein from *E. coli* and *Salmonella* (19, 20). ZinT has been implicated in aiding Zn^{2+} uptake, but how this is achieved has remained unclear (19, 20). The $AdcA_C$ domain is linked to the N-terminal cluster A-I domain of AdcA (residues 1 to 311, henceforth referred to as $AdcA_N$) by an 11-amino-acid linking region (3, 14). $AdcA_N$ also has an additional structural feature absent from AdcAII, a region enriched with histidine and glutamate residues (residues 120 to 136, referred to as the His-rich loop). His-rich loops are prevalent in Zn^{2+}-specific SBPs, although their contribution to Zn^{2+} recruitment also remains poorly defined (21, 22). Thus, AdcA is comprised of various structural elements implicated in Zn^{2+} acquisition, but how they collectively serve in this process is unknown.

To date, high-resolution crystal structures have only been determined for single domain SBPs from Gram-negative organisms, while two-domain SBPs have remained refractory to such approaches (21, 23, 24). Further, although crystal structures have been solved in the presence or absence of a metal ion, the minor changes in tertiary structure coupled with a lack of insight into protein dynamics have limited mechanistic insight into how Zn^{2+}-specific SBPs achieve selection for Zn^{2+} ions. Here, we combined high-resolution structural analyses, molecular dynamics (MD) simulations, and electron paramagnetic resonance (EPR) studies to elucidate the molecular basis of Zn^{2+} acquisition in AdcA. We report the first high-resolution structure of a Zn^{2+}-bound two-domain SBP, AdcA, and reveal the essential role of the $AdcA_N$ domain in pneumococcal Zn^{2+} uptake and the relative contributions of the "accessory" regions (His-rich loop and $AdcA_C$ domain) to this process. We then investigate the conformational landscape of

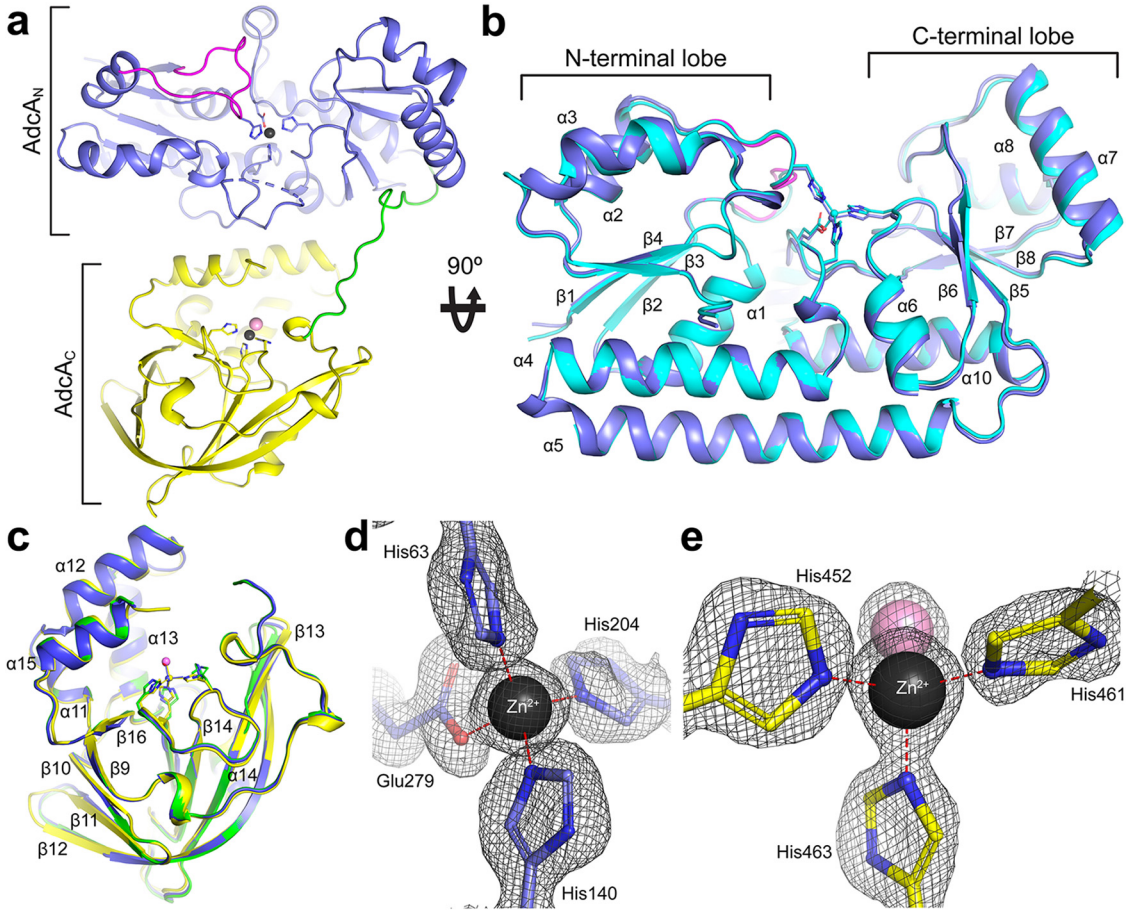

FIG 1 Structure of AdcA. (a) Cartoon representation of the AdcA crystal structure. The AdcA$_N$ domain is colored in light blue, and the AdcA$_C$ domain is colored in yellow. The bound Zn^{2+} ions are shown as black spheres, with their coordinating residues shown as sticks. The Cl^- ion coordinating the Zn^{2+} in the AdcA$_C$ domain is shown as a pink sphere. The domain-linking loop is colored in green. The missing residues in the His-rich loop are indicated by a dashed line. The loop $\alpha 2\beta 2$ is colored in magenta. (b) Superposition of the crystal structures of the AdcA$_N$ domain from full-length AdcA (light blue) and AdcA$_N$ expressed on its own (cyan), viewed from a 90° rotation from the orientation depicted in panel a. The bound Zn^{2+} ions are shown as spheres, with their colors matching the respective structures. The Zn^{2+} coordinating residues are shown as sticks. The coordination bonds are illustrated with dotted lines. (c) Superposition of the crystal structure of the AdcA$_C$ domain from full-length AdcA (yellow) with the crystal structures of AdcA$_C$ expressed on its own (metal-free, green; Zn^{2+}-bound, blue), viewed from the same orientation depicted in panel a. The bound Zn^{2+} are shown as spheres, with their colors matching the respective structures. The Zn^{2+} coordinating residues are shown as sticks. The pink sphere represents the Cl^- that is bound to the Zn^{2+} in the AdcA$_C$ domain. The coordination bonds are illustrated with dotted lines. (d and e) Close-up views of the metal-binding sites in the AdcA$_N$ and AdcA$_C$ domains, respectively. The bound Zn^{2+} ions are presented as black spheres, and the coordinating residues are presented as sticks. The coordination bonds are indicated by dashed red lines. The $2F_o$-F_c electron density map, contoured at 1.5 σ, is shown in gray mesh presentation.

the AdcA$_N$ domain and show that ligand-binding induces only localized structural rearrangements within this domain. A key structural element within the AdcA$_N$ domain is surface loop $\alpha 2\beta 2$, a highly dynamic region that is stabilized by ligand-binding in a process crucial for AdcCB-mediated Zn^{2+} uptake. Collectively, these findings provide new mechanistic insight into how Zn^{2+}-specific cluster A-I SBPs bind metal ligands and the structural elements that contribute to bacterial Zn^{2+} import. These findings provide a structural framework for the development of novel inhibitors targeting AdcA against pneumococcal infections.

RESULTS

Structure of Zn^{2+}-bound AdcA. The high-resolution crystal structure of wild-type, Zn^{2+}-bound AdcA was determined at 1.58-Å resolution and revealed a two-domain organization with the AdcA$_N$ and AdcA$_C$ domains forming discrete globular regions, connected by an 11-amino-acid linker and each containing one Zn^{2+} ion (Fig. 1a to c; see

TABLE 1 Effect of transition metal ions on the melting temperature of AdcA and truncated variants[a]

	AdcA		$AdcA_N$		$AdcA_C$	
Treatment	T_m (°C)	ΔT_m (°C)	T_m (°C)	ΔT_m (°C)	T_m (°C)	ΔT_m (°C)
Metal-free	52.51 ± 0.56		40.74 ± 0.68		54.64 ± 0.50	
Mn^{2+}	52.19 ± 0.31	–0.32	40.10 ± 0.02	–0.64	56.31 ± 0.97	+1.67
Fe^{2+}	54.55 ± 2.80	+2.04	39.40 ± 0.11	–1.34	55.66 ± 0.16	+1.02
Co^{2+}	59.93 ± 1.23	+7.42*	38.93 ± 0.06	–1.81	62.85 ± 1.05	+8.21*
Ni^{2+}	60.40 ± 0.65	+7.89*	40.34 ± 0.06	–0.40	63.54 ± 2.13	+8.90*
Cu^{2+}	57.57 ± 0.69	+5.06	39.40 ± 0.22	–1.34	57.24 ± 1.12	+2.60
Zn^{2+}	66.35 ± 1.78	+13.84*	63.83 ± 0.06	+23.09*	67.80 ± 2.01	+13.16*

[a]The T_m values represent averages and standard errors of the mean for at least three independent measurements. *, Statistically significant difference compared to metal-free protein T_m (calculated using one-way ANOVA with Tukey's posttest).

also Fig. S1, Fig. S2, and Table S1 in the supplemental material). The $AdcA_N$ domain has a two-lobed organization, with the N- and C-terminal $(\alpha/\beta)_4$ lobes bisected by a cleft in which the metal binds. The binding site in $AdcA_N$ is comprised of three Nε2 atoms from His63, His140, and His204 and one Oε2 atom from Glu279. These four residues bind a single Zn^{2+} ion via 4-coordinate geometry, with bond distances of 1.98 to 2.08 Å (Fig. 1d). MD simulations analyzing the stability of the bond distances for the metal-coordinating residues showed that these distances remained stable, averaging 2.07 to 2.15 Å over five independent 750-ns simulations, consistent with Zn^{2+} coordination by proteins (25). Metal binding was restricted to Zn^{2+} ions, with differential scanning fluorimetry (DSF) showing that other divalent first-row transition metal ions did not induce stabilization of the N-terminal domain (Table 1).

Electron density was not observed for 14 residues (120 to 133) of the His-rich loop, consistent with the predicted flexibility of this region (26, 27). The two lobes of the $AdcA_N$ domain are linked by a rigid α-helix (α5). This fold is highly conserved among cluster A-I SBPs, including *S. pneumoniae* AdcAII (PDB 3CX3; Cα root mean square deviation [RMSD], 0.91 Å), *Salmonella enterica* ZnuA (PDB 2XY4; Cα RMSD, 1.78 Å), and *S. pneumoniae* PsaA (PDB 3ZTT; Cα RMSD, 1.36 Å) (see Fig. S1B in the supplemental material). Intriguingly, the $AdcA_N$ domain was observed in a conformation that partially exposed the metal-binding site to bulk solvent, with the relative solvent accessibility of the metal-binding residues (His63 > His140 > His204 ≈ Glu279) remaining the same during the five independent MD simulations. This partial open conformation was also observed in the *S. enterica* Zn^{2+}-bound ZnuA structures (27). However, in other Zn^{2+}-bound ZnuA crystal structures, the Zn^{2+}-binding sites adopted a fully closed conformation (21, 22, 26). The partial opening of the Zn^{2+}-binding site of the $AdcA_N$ domain arises from the $\alpha7\beta6$ loop having moved away from the binding site due to rigid-body rotational movements of α7 in a plane perpendicular to the helical hinge interlobe helix α5. This conformation was also observed for the truncated AdcA variant that lacked $AdcA_C$, $AdcA_N$ (residues 27 to 309). The high-resolution crystal structure of Zn^{2+}-bound truncated $AdcA_N$ (Fig. 1b; see also Fig. S1C and Table S1) did not reveal any conformational differences by comparison with the N-terminal domain of the full-length, wild-type protein.

The $AdcA_C$ domain has a lipocalin-like fold of an 8-stranded up-and-down β-barrel (β9-16) and a helical region of four short helices (α11 to α15) (Fig. 1c; see also Fig. S2A). The Zn^{2+}-binding site of the $AdcA_C$ domain is formed by three Nε2 atoms from His452, His461, and His463 binding a single Zn^{2+} ion with bond distances of 1.97 to 2.11 Å (Fig. 1e). These bond distances remained stable over five independent MD simulations. The metal-binding site of the $AdcA_C$ domain showed greater promiscuity than the $AdcA_N$ domain, with Co^{2+} and Ni^{2+} inducing protein stabilization, albeit to a lesser extent than Zn^{2+} (Table 1). The overall fold of the $AdcA_C$ domain closely resembles the ZinT family of proteins from Gram-negative bacteria, such as *E. coli* (PDB 1OEK;

Cα RMSD, 0.63 Å) and *S. enterica* (PDB 4AYH; Cα RMSD, 0.58 Å) (see Fig. S2B). The structure of the $AdcA_C$ domain was further analyzed compared to a truncated AdcA variant lacking $AdcA_N$, $AdcA_C$ (residues 326 to 501). The high-resolution crystal structure of isolated Zn^{2+}-bound truncated $AdcA_C$ did not reveal any conformational differences by comparison with the domain present in the full-length protein (Fig. 1c; see also Fig. S2C and Table S1). The structure of metal-free truncated $AdcA_C$ (see Table S1) was also determined, showing that only minor conformational changes are induced by metal binding (Fig. 1c; see also Fig. S2C). These observations are consistent with MD simulations of metal-free and Zn^{2+}-bound AdcA; comparisons of Cα RMSD over time showed no significant structural differences between the simulations of the protein in the two states (see Table S2A and Text S1A).

In Zn^{2+}-bound AdcA, interaction between the domains occurs between α12 and α15 of the $AdcA_C$ domain and α7 and the base portion of the His-rich loop (residues 109 to 117) of the $AdcA_N$ domain, with a buried surface area of ~1,200 Å^2. An extensive array of intramolecular interactions was observed at the interface of the two domains. MD analyses suggest that the most stable portion of the interface arises from interactions between six residues from each domain. The most stable part of the interface involves the salt bridge between Lys368 and Asp213 and H-bonds formed by the side chain of Tyr365 with the backbone and side chain of Asp213 and the backbone of Leu212. Residues Gln492 and Gln496 also form a stable part of the interface, but their interacting residues are dependent upon protein conformation. Gln492 alternates between forming H-bonds with the backbone of Leu115 and the side chain of Asp112. The side chain of Gln496 interacts with both the aromatic ring of Phe137 and the backbone of Leu115. Similarly, Glu120 in the $AdcA_N$ domain forms a salt bridge with Lys318, as well as H-bonds with the imidazole ring of His501 in the $AdcA_C$ domain, depending on the conformation of the protein. The interactions between these residues define a relatively large and stable buried surface area via a combination of salt bridges, H bonding, and transient interactions. The stability of these interactions and average distances are provided in Table S2B. We then sought to understand how the structural features of AdcA contributed to pneumococcal Zn^{2+} acquisition.

Zinc acquisition requires the $AdcA_N$ domain. The role of the $AdcA_N$ domain was investigated using mutant variants of AdcA wherein the N-terminal domain was deleted (*adcA*$_C$) or the Zn^{2+}-coordinating His residues (His63, His140, and His204) were mutated to Ala (*adcA*$_{\Delta His}$), thereby abolishing its Zn^{2+}-binding capacity. The contribution of $AdcA_N$ to Zn^{2+} uptake was then assessed in the *S. pneumoniae* Δ*adcAII* background. The resultant strains (Δ*adcAII* Δ*adcA*::*adcA*$_C$ and Δ*adcAII* Δ*adcA*::*adcA*$_{\Delta His}$) showed a significant growth defect in Zn^{2+}-restricted conditions ($P < 0.0001$, one-way analysis of variance [ANOVA]) and had a growth profile in Zn^{2+}-replete media similar to that of the Δ*adcA* Δ*adcAII* deletion strain, wherein Adc permease function is abrogated (Fig. 2a; see also Fig. S3). Accumulation of Zn^{2+} in the mutant strains was also significantly impaired in both Zn^{2+}-replete and Zn^{2+}-restricted media (Fig. 2b and c; see also Fig. S4), with no other transition metal ions showing impaired accumulation (Fig. 2b and c; see also Fig. S4). Taken together, these data show that the $AdcA_N$ domain is necessary for pneumococcal Zn^{2+} acquisition.

The $AdcA_C$ domain and His-rich loop aid in zinc uptake. We then investigated the contributions of the $AdcA_C$ domain and the His-rich loop of the $AdcA_N$ domain (residues 120 to 136) in Zn^{2+} uptake. AdcA variants were generated in which (i) the $AdcA_C$ domain was truncated (*adcA*$_N$), (ii) the His-rich loop was deleted (*adcA*$_{\Delta Loop}$), or (iii) both $AdcA_C$ and the His-rich loop were deleted (*adcA*$_{N\Delta Loop}$). In the Δ*adcAII* background, deletion of either accessory region had no significant impact on growth in Zn^{2+}-restricted conditions, compared to Zn^{2+}-replete conditions (Fig. 2a; see also Fig. S3). However, loss of both accessory regions (*adcA*$_{N\Delta Loop}$ strain) resulted in a significant growth defect under Zn^{2+}-restriction (Fig. 2a; see also Fig. S3). Zinc accumulation in the *adcA*$_{N\Delta Loop}$ strain was only impaired during growth under Zn^{2+} restriction, while accumulation of other ions was unaffected (Fig. 2b and c; see also Fig. S4). Collectively, our data show that the $AdcA_N$ domain is necessary and sufficient for Zn^{2+} acquisition, with the $AdcA_C$

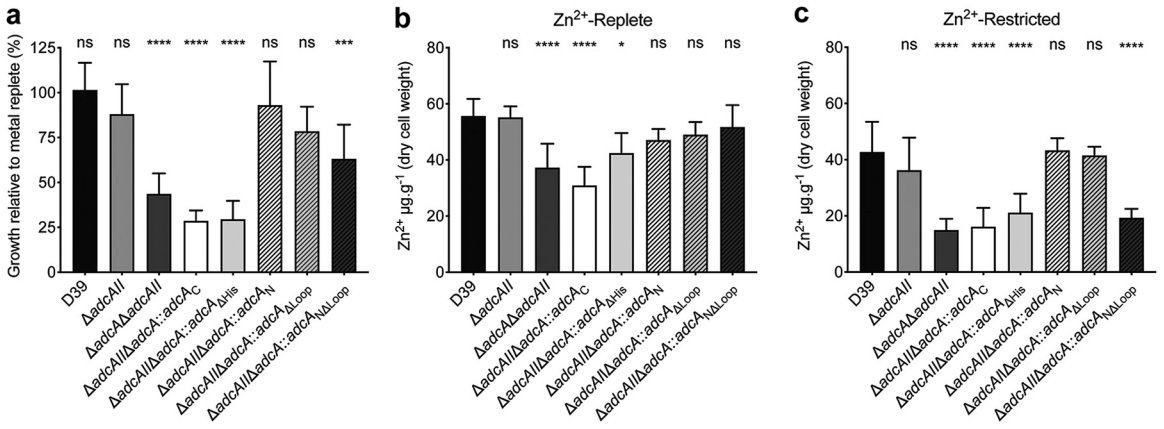

FIG 2 AdcA facilitates growth under Zn^{2+}-limiting conditions. (a) *In vitro* growth yields of wild-type *S. pneumoniae* D39 and the *adc* mutant strains. Bacteria were grown in CDM, with or without treatment with the preferential zinc chelator TPEN (*N*,*N*,*N*′,*N*′-tetrakis(2-pyridinylmethyl)-1,2-ethanediamine). The data are representative mean (± the SEM) optical density at 600 nm (OD_{600}) measurements at 300 min from at least three independent biological experiments, normalized to growth in Zn^{2+}-replete conditions. Statistical significance of the differences in growth compared to wild-type bacteria was determined by a one-way ANOVA with Tukey posttest. *P* values of <0.005 and <0.0001 are denoted by asterisks (*** or ****, respectively). (b and c) Intracellular Zn^{2+} accumulation of *S. pneumoniae* D39 and the *adc* mutant strains in CDM in the absence (b) or presence (c) of TPEN supplementation, as determined by ICP-MS. Data correspond to mean (± the SEM) μg Zn^{2+} g^{-1} cell measurements from three independent biological experiments. The statistical significance of the differences in concentrations was determined by using one-way ANOVA with the Tukey posttest. *P* values of <0.05 and <0.0001 are denoted by asterisks (* or ****, respectively). ns, not significant.

domain and the His-rich loop aiding in Zn^{2+} recruitment during growth under Zn^{2+}-restricted conditions. Therefore, it logically follows that Zn^{2+} uptake in the Adc permease is regulated by the $AdcA_N$ domain of AdcA.

Zinc binding induces localized conformational changes. Ligand binding in SBPs is generally associated with protein conformational changes, although the extent of rearrangement varies depending on the intrinsic flexibility of the protein and the identity of ligand(s) (15). Formation of an SBP-ligand complex is a prerequisite for ABC permease-mediated import. We investigated the influence of Zn^{2+}-binding on the conformation of the $AdcA_N$ domain to determine whether it contributed as a mechanistic determinant in regulating Zn^{2+} uptake. Due to the paucity of mechanistic information on a Zn^{2+}-binding mechanism for cluster A-I SBPs, we initially compared AdcA with the cluster A-I manganese (Mn^{2+}) ion-recruiting SBP PsaA, for which a ligand-binding mechanism and the relationship of this mechanism to cation import have been reported (18, 28). In PsaA, ligand binding induces the closure of the metal-binding site, facilitated by partial unwinding of the lobe-linking α-helix and the breakage of H-bonds between main-chain N and O atoms in the helix, and relatively large movement of the C-terminal lobe. These movements are reflected by the high root mean square fluctuations (RMSF) in MD simulations (18). Given the similarity in the protein sequence (51% identity across 313 residues) and function, we investigated whether the $AdcA_N$ domain used a similar mechanism. Analysis of the residues in the C-terminal lobe of the $AdcA_N$ domain, corresponding to those associated with the mechanism in PsaA (residues 225 to 250), revealed that they did not exhibit high RMSF values. Further, examination of the H-bond network of the lobe-linking α-helix (α5, residues 167 to 193) region in Zn^{2+}-bound $AdcA_N$ showed that all H-bond lengths were $\sim$3 Å, the ideal range for a helical conformation (29), and the majority (19 of 25 of H-bonds) were present for $\geq$95% of the simulation time, with a mean distance of $\sim 2.0 \pm 0.2$ Å (see Table S2C). Thus, the α-helix appeared stable, with H-bond networks unaffected by metal occupancy status of the protein. These data suggest that the metal-binding mechanism is not associated with a distortion of the lobe-linking α-helix or a large-scale movement of the SBP lobes, indicating a distinct ligand-binding mechanism.

The conformational plasticity of the $AdcA_N$ domain was then directly examined

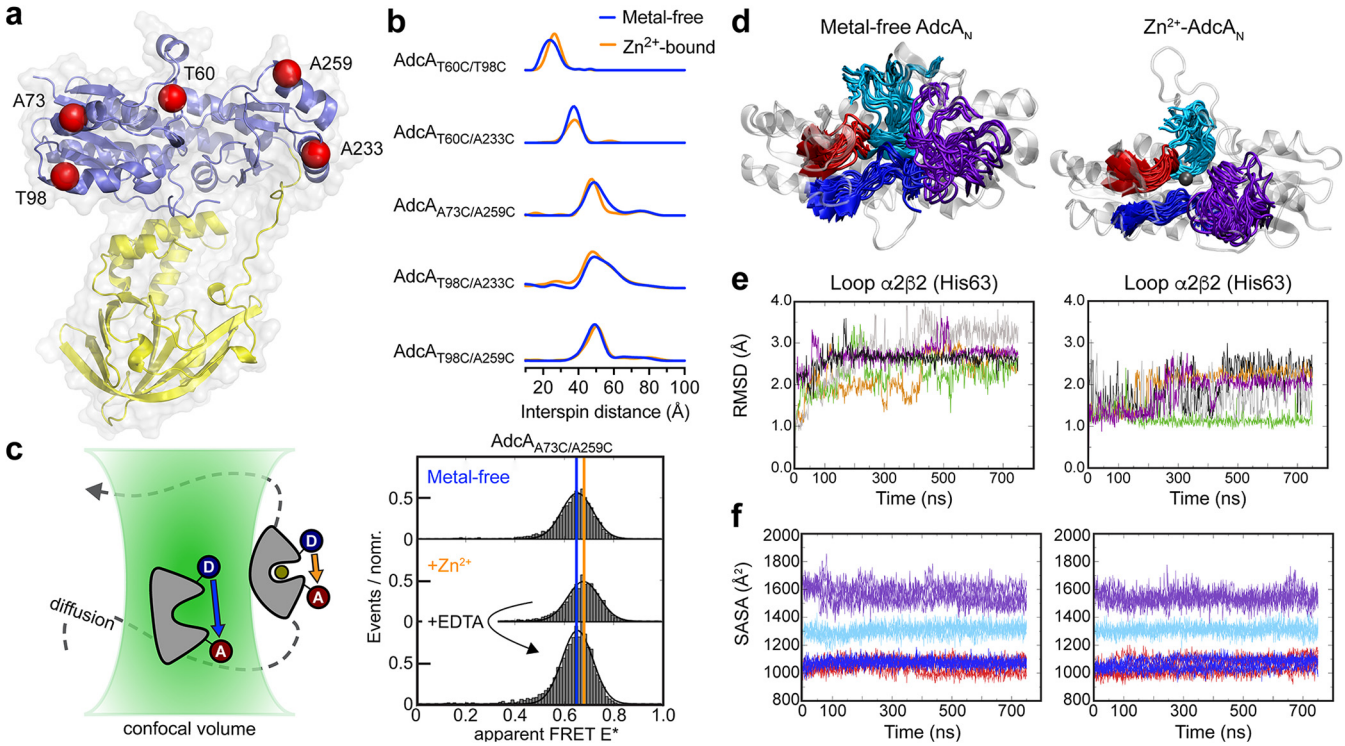

FIG 3 Biophysical and computational analyses of AdcA. (a) Cartoon representation of AdcA, with the five residues mutated to cysteine shown as red spheres. (b) Metal-free (blue) and Zn^{2+}-bound (orange) MTSSL-labeled AdcA-Cys variants analyzed by Q-band DEER data, with the distance distributions computed using Tikhonov regularization (see Text S1C). (c) Scheme of the experimental setup for smFRET microscopy of AdcA molecules with donor (D) and acceptor (A). Projections of E* are shown for $AdcA_{A73C/A259C}$ in the metal-free state (blue line; 50 μM EDTA), Zn^{2+}-bound state (orange line; 100 μM Zn^{2+}) and in the presence of excess EDTA (100 μM Zn^{2+} plus 1 mM EDTA) with fits. (d) $AdcA_N$ in the metal-free and Zn^{2+}-bound state with snapshots of the four metal-binding residue-containing loops obtained from MD simulations. $AdcA_N$ is shown as a cartoon representation (white), with Zn^{2+} as a sphere (black) and the metal-binding residue-containing loops shown in different colors: loop $\alpha 2\beta 2$ (residues 55 to 65; His63) in purple, loop $\alpha 4\beta 4$ (residues 135 to 144; His140) in cyan, loop $\alpha 6\beta 5$ (residues 201 to 207; His204) in red, and loop $\alpha 10\beta 8$ (residues 274 to 281; Glu279) in blue. (e) RMSD analysis of loop $\alpha 2\beta 2$, which contains His63, in the metal-free and Zn^{2+}-bound state, with individual trajectories represented by the different colors. RMSD analyses of the other loops are presented in Table 4. (f) Solvent accessible surface area (SASA) over time for the four loops ($\alpha 2\beta 2$, $\alpha 4\beta 4$, $\alpha 6\beta 5$, and $\alpha 10\beta 8$) from the five independent simulations of metal-free and Zn^{2+}-bound AdcA, using the loop color scheme in panel d.

using double electron-electron resonance (DEER) spectroscopy. Five full-length AdcA variants were generated, by combining pairs of Cys residues in the N-terminal domain of the protein, each of which was analyzed in the metal-free and Zn^{2+}-bound states (Fig. 3a). DSF analyses indicated that introduction of the Cys-residues had no impact on Zn^{2+}-binding by the AdcA variants (Table 2). DEER determination of the mean NO•-NO• distances and widths in Zn^{2+}-bound AdcA-Cys variants correlated closely with crystal structure analyses (Fig. 3b and Table 3; see also Text S1B). Nonetheless, the DEER distance distribution widths were slightly greater, suggesting that the protein is

TABLE 2 Effect of zinc on the melting temperature of AdcA variants

Sample	Mean T_m (°C) ± SEM[a]	ΔT_m (°C)[b]
Metal-free $AdcA_{T60C/T98C}$	51.26 ± 0.43	
Zn^{2+}-$AdcA_{T60C/T98C}$	69.94 ± 0.50	+18.68*
Metal-free $AdcA_{T60C/A233C}$	49.14 ± 1.82	
Zn^{2+}-$AdcA_{T60C/A233C}$	68.17 ± 0.50	+19.03*
Metal-free $AdcA_{A73C/A259C}$	48.47 ± 0.47	
Zn^{2+}-$AdcA_{A73C/A259C}$	69.60 ± 0.47	+21.13*
Metal-free $AdcA_{T98C/A233C}$	47.37 ± 0.44	
Zn^{2+}-$AdcA_{T98C/A233C}$	68.51 ± 1.04	+21.14*
Metal-free $AdcA_{T98C/A259C}$	49.54 ± 0.74	
Zn^{2+}-$AdcA_{T98C/A259C}$	68.64 ± 0.50	+20.05*

[a]The values shown represent averages from at least four independent measurements.
[b]*, Statistically significant difference compared to the respective metal-free AdcA cysteine variant T_m (one-way ANOVA with Dunnett's posttest).

TABLE 3 Inter-residue distance analyses of AdcA

	C_α-C_α distance (Å) ± the SD		r_{DD}/σ_{DD} (Å)[c]	
Protein	MD[a]	MD-DEER[b]	DD-crystal	DD-DEER
Metal-free $AdcA_{T60C/T98C}$	22.5 ± 5.8	23.2 ± 6.1		24.9/5.3
Zn^{2+}-$AdcA_{T60C/T98C}$	27.7 ± 4.3	21.8 ± 3.8	26.2/5.5	26.5/4.8
Metal-free $AdcA_{T60C/A233C}$	32.7 ± 4.8	33.6 ± 4.5		37.2/3.4
Zn^{2+}-$AdcA_{T60C/A233C}$	28.7 ± 3.7	31.5 ± 2.8	34.8/6.4	38.1/6.8
Metal-free $AdcA_{A73C/A259C}$	45.8 ± 3.5	45.4 ± 3.2		52.5/11.1
Zn^{2+}-$AdcA_{A73C/A259C}$	44.2 ± 3.1	43.1 ± 2.8	46.6/5.9	49.9/12.1
Metal-free $AdcA_{T98C/A233C}$	46.8 ± 4.5	53.9 ± 5.3		55.4/12.8
Zn^{2+}-$AdcA_{T98C/A233C}$	49.9 ± 6.6	50.1 ± 5.4	48.7/6.4	51.8/12.6
Metal-free $AdcA_{T98C/A259C}$	44.7 ± 4.5	52.8 ± 5.4		53.2/17.5
Zn^{2+}-$AdcA_{T98C/A259C}$	49.4 ± 6.8	48.2 ± 4.9	49.9/5.9	51.6/15.3

[a]Calculated mean Cα-Cα distance from the last 250 ns of the five 750-ns MD simulations of AdcA in the metal-bound or metal-free state, as indicated.
[b]Calculated mean Cα-Cα distances from the set of MD structures that optimally model the DEER data.
[c]r_{DD} is the mean NO•-NO• interresidue distance (Å), and σ_{DD} is the width of the DEER distance distribution (DD).

slightly more conformationally dynamic in frozen solution. Comparisons of the metal-free and Zn^{2+}-bound states of the AdcA-Cys variants revealed only small changes (<4 Å) in the mean distance distributions, as well as small changes in the distance distribution widths (Fig. 3b; see also Fig. S5). We then compared the experimental DEER data with our MD analyses, by deriving an MD structural model of metal-free and Zn^{2+}-bound AdcA to describe the DEER data. This was achieved using the complete set of MD trajectories (see Fig. S6A to E) that was then refined to a subset that best fitted the experimental data, resulting in excellent agreement between experiment and model data (Fig. 3b and Table 3; see also Fig. S6F to J). Comparison of the full set of MD simulations computed at room temperature with the subset that optimally describes the frozen-solution DEER data showed that both data sets sampled highly similar conformational landscapes (see Fig. S6K and L). Thus, the experimental DEER data and MD analyses both showed that Zn^{2+}-binding in the $AdcA_N$ domain induces only minor changes in global protein conformation. To complement these analyses, we investigated full-length $AdcA_{A73C/A259C}$ by smFRET, since the inter-residue distances were compatible with the technique (Fig. 3c). Freely diffusing, fluorophore-labeled $AdcA_{A73C/A259C}$ showed that Zn^{2+}-binding induced only a minor change in the apparent FRET efficiency (metal-free E* = 0.65; Zn^{2+}-bound E* = 0.68; Fig. 3c) consistent with the DEER and MD observations and similar to our previous smFRET analyses of the SBP PsaA (28). We then investigated the influence of Zn^{2+} on the conformational dynamics of ligand release from AdcA. Here, addition of the divalent-metal chelating compound EDTA immediately removed Zn^{2+} from the $AdcA_N$ domain, as shown by return to the apparent FRET efficiencies of the metal-free protein (Fig. 3c). These data indicate that the Zn^{2+}-bound conformation of AdcA is able to readily release Zn^{2+} from the high-affinity site in the $AdcA_N$ domain to bulk solvent, and thus the lifetime of the $AdcA_N$-Zn^{2+} complex is shorter than a few seconds.

Collectively, these findings show, for the first time, that Zn^{2+} binding induces only minor changes in the global conformation of AdcA in solution, with the resultant protein-metal complex able to efficiently release bound Zn^{2+} ions. Nevertheless, the ligand-free conformations of AdcA and the $AdcA_N$ domain were refractory to crystallization, suggesting that ligand-binding was required to stabilize surface protein dynamics. Thus, we examined the surface dynamics of the $AdcA_N$ domain to elucidate their contribution to the Zn^{2+}-binding mechanism of the protein.

Loop $\alpha 2\beta 2$ is a dynamic structural element within $AdcA_N$. The loops containing the metal-coordinating residues are the regions in the $AdcA_N$ domain most likely to contain structural elements influenced by Zn^{2+} binding. MD simulations were used to analyze loop mobility, assessed using RMSD and the solvent accessible surface area (SASA) as a function of time in the presence and absence of Zn^{2+} (Fig. 3d to f and Table 4). This

TABLE 4 MD analysis of the $AdcA_N$ domain loops containing metal-coordinating residues

	Mean RMSD (Å) ± the SD[a]	
AdcA loop	Metal-free AdcA	Zn^{2+}-bound AdcA
Loop $\alpha2\beta2$ (residues 55–65; His63)	2.7 ± 0.3*	1.9 ± 0.4*
Loop $\alpha4\beta4$ (residues 135–144; His140)	1.3 ± 0.3	1.3 ± 0.3
Loop $\alpha6\beta5$ (residues 201–207; His204)	2.0 ± 0.2	1.7 ± 0.3
Loop $\alpha10\beta8$ (residues 274–281; Glu279)	2.0 ± 0.3	1.6 ± 0.4

[a]Values shown represent the average Cα RMSD for the $AdcA_N$ domain loops containing the metal-binding residues and were calculated by combining the frames from the last 250 ns of each of the five independent 750-ns MD simulations of metal-free and Zn^{2+}-bound AdcA, respectively (the data set). The RMSD values were calculated using the starting structure of the simulation as a reference and averaged over the data set. *, Statistically significant difference, based on a 68% confidence interval.

revealed that loop $\alpha2\beta2$, which contains His63, had the highest mobility and solvent accessibility of the four regions in the metal-free and Zn^{2+}-bound states of AdcA (Fig. 3d to f and Table 4). Further, it was the only region to have a significant difference in mobility between the metal-free and Zn^{2+}-bound states (Table 4). In contrast, although loop $\alpha6\beta5$ (His204) showed some mobility, it did not significantly differ between the metal-free and Zn^{2+}-bound states. Loops $\alpha10\beta8$ (Glu279) and $\alpha4\beta4$ (His140) showed low mobility in either state. These data suggest that His140, His204, and Glu279 provide a largely preformed metal-binding site, with loop $\alpha2\beta2$ (His63) acting as a region of dynamic mobility that is stabilized by Zn^{2+} binding.

To verify the MD analysis, we investigated the mobility of loop $\alpha2\beta2$ in solution, using X-band continuous-wave EPR. Two single AdcA-Cys variants, $AdcA_{T60C}$ (located on loop $\alpha2\beta2$) and $AdcA_{T98C}$ (located on helix $\alpha3$), were examined in the presence and absence of Zn^{2+}. We observed that the MTSSL label was more mobile in $AdcA_{T60C}$, by comparison with $AdcA_{T98C}$ (see Fig. S6M), consistent with MD analyses based on RMSD values of these two residues. Upon Zn^{2+} binding, the motility of the MTSSL label on $AdcA_{T60C}$ was reduced to a greater extent than the one on $AdcA_{T98C}$ (see Fig. S6M), consistent with loop $\alpha2\beta2$ experiencing a mobility change in response to Zn^{2+}-binding. Taken together, these findings indicate that the dynamics of the loop $\alpha2\beta2$ are directly influenced by Zn^{2+} binding.

Role of loop $\alpha2\beta2$ in zinc acquisition. We next investigated the contribution of loop $\alpha2\beta2$ in Zn^{2+} acquisition by introducing a H63A mutation to uncouple loop stabilization from Zn^{2+} binding. Mutation of the metal-binding site residue reduced affinity for Zn^{2+}, relative to the wild-type protein (3), but was comparable to the impact mediated by mutation of another binding site residue, H204A (Table 5). Introduction of the mutant alleles into *S. pneumoniae* significantly impacted growth of the Δ*adcAII* Δ*adcA*::$adcA_{H63A}$ strain in Zn^{2+}-restricted media, relative to the wild-type and Δ*adcAII* strains, but not the Δ*adcAII* Δ*adcA*::$adcA_{H204A}$ strain (Fig. 4a). Consistent with the phenotypic growth impact conferred by the mutation of His63, pneumococcal Zn^{2+} accumulation was also reduced in the *adcAII* Δ*adcA*::$adcA_{H63A}$ strain, relative to the wild-type strain (Fig. 4b). Thus, while both His63 and His204 contribute to the affinity of AdcA for Zn^{2+} binding, these data indicate that stabilization of loop $\alpha2\beta2$ via His63 also contributes to the efficacy of bacterial Zn^{2+} uptake. Taken together, we propose that the dynamic mobility of loop $\alpha2\beta2$ contributes to productive interaction of ligand-bound AdcA with the AdcCB transporter to facilitate Zn^{2+} translocation. The molecular details of the SBP-transporter interaction and how it contributes to Zn^{2+} release and import warrant further investigation.

TABLE 5 Affinity analyses of truncated $AdcA_N$ variants

$AdcA_N$ variant	Mean derived K_d (M) ± the SEM[a]
H63A	$(4.32 \pm 0.8) \times 10^{-7}$
H204A	$(5.99 \pm 1.3) \times 10^{-7}$

[a]Values represent the means of four replicates.

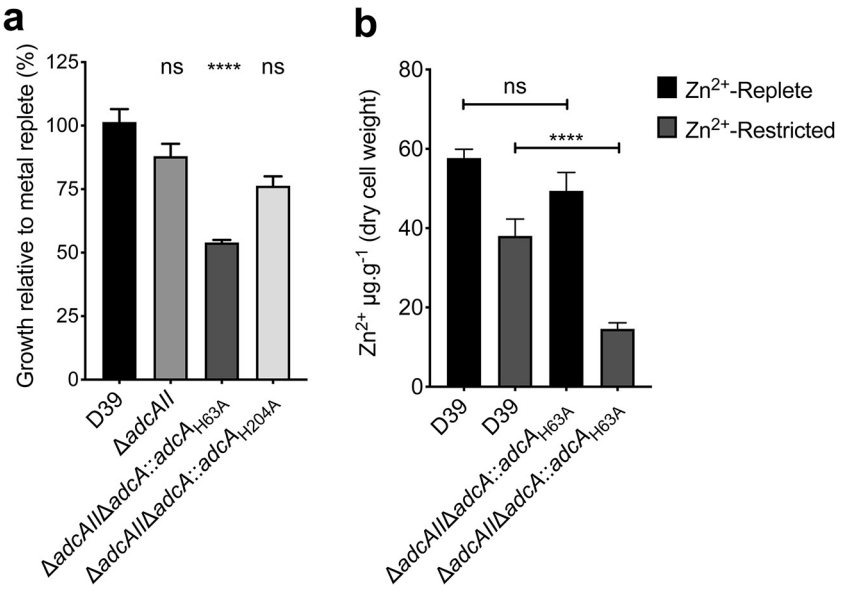

FIG 4 Mutation of His63 impacts Zn^{2+} accumulation. (a) *In vitro* growth measurements of wild-type *S. pneumoniae* D39 and the Δ*adcAII*, Δ*adcAII* Δ*adcA*::*adcA*$_{H63A}$, and Δ*adcAII* Δ*adcA*::*adcA*$_{H204A}$ mutant strains. Bacteria were grown in CDM, with or without treatment with TPEN, and incubated at 37°C and 5% CO_2 with growth monitored by optical density (OD_{600}) measurements. The data are representative mean (± the SEM) OD_{600} measurements at 300 min from at least three independent biological experiments, normalized to growth in Zn^{2+}-replete conditions. The statistical significance of the differences in growth compared to the wild-type strain was determined by a one-way ANOVA, with the Tukey posttest. *P* values of <0.0001 are denoted by asterisks (****). (b) *In vitro* Zn^{2+} accumulation of wild-type *S. pneumoniae* D39 and Δ*adcAII* Δ*adcA*::*adcA*$_{H63A}$, grown in Zn^{2+}-replete or -restricted medium assessed by ICP-MS. The data correspond to the mean (± the SEM) μg metal g^{-1} (dry cell weight) from three measurements in two independent biological experiments. Statistical significance was determined by using one-way ANOVA with the Tukey posttest. *P* values of <0.0001 are denoted by asterisks (****). ns, not significant.

Proposed binding mechanism of AdcA. Collectively, our biochemical, biophysical, and structural analyses reveal how Zn^{2+}-specific SBPs selectively acquire Zn^{2+} ions and the contribution of a mobile surface loop ($\alpha2\beta2$) in facilitating bacterial metal uptake. In AdcA, the solvent-accessible accessory regions, i.e. the His-rich loop and the $AdcA_C$ domain, serve to aid in Zn^{2+} recruitment from bulk solvent and increase its availability to $AdcA_N$. Ligand binding in the $AdcA_N$ domain occurs at a preformed, relatively static metal-binding site and, although not associated with global changes in protein conformation, stabilizes the surface loop $\alpha2\beta2$. In metal-free AdcA, loop $\alpha2\beta2$ is highly mobile and increases the solvent accessibility of the metal-binding site. Upon interaction with Zn^{2+}, the metal-coordinating residue His63, contained within loop $\alpha2\beta2$, initiates closure of the metal-binding site as the loop is pulled onto the binding site, thereby decreasing solvent accessibility. The concomitant reduction in loop $\alpha2\beta2$ mobility stabilizes the $AdcA_N$ surface. Zinc-bound AdcA is then able to productively interact with the cognate AdcCB transporter and release the bound metal into the translocation pathway. The molecular details of the interaction between AdcA and AdcB and how Zn^{2+} is released to the transporter remain to be elucidated. These structural features, which can be summarized as a limited conformational landscape, a rigid metal-binding site, and a flexible surface loop, appear to be well conserved among Zn^{2+}-specific SBPs, suggesting a common mechanistic basis for prokaryotic Zn^{2+} uptake (26, 30). In summary, the metal-binding mechanism in AdcA is akin to a "trap-door," in which the protein conformational changes can be summarized as a mobile region (loop $\alpha2\beta2$, "open trap-door") that pushes onto a largely static metal-binding site (His140, His204 and Glu279), closing ("shut trap-door") upon metal binding.

DISCUSSION

This study defines a structural basis for selective Zn^{2+} acquisition by two-domain lipoproteins in bacterial ABC importers. Our findings show that the $AdcA_N$ domain of AdcA is necessary and sufficient for Zn^{2+} import, with ligand binding stabilizing the dynamic loop $\alpha 2\beta 2$. This conformational change contributes to the efficacy of bacterial Zn^{2+} uptake, highlighting the link between ligand-induced conformational changes and the translocation competency of two-domain Zn^{2+}-recruiting SBPs. Our mechanism is also consistent with the structural observations with the $AdcA_N$ homologs ZnuA from *E. coli* (26) and SitA from *Staphylococcus pseudintermedius* (30). Although those studies lacked insight into protein conformational dynamics and Zn^{2+} transport, an analysis of the structural data showed localized conformational rearrangements accompanied by alterations in the flexibility of the loop region containing the residue equivalent to His63. Thus, our findings explain the significance of the Zn^{2+}-induced restriction of loop $\alpha 2\beta 2$ mobility. The coupling of ligand-induced localized conformational changes to facile interaction with an ABC transporter is not unprecedented (31). However, it is important to note that the highly localized structural rearrangements in AdcA and other Zn^{2+}-specific SBPs are toward the minimal end of the conformational landscape that could facilitate such a process. This is most likely attributable to the structural elements that define the metal-binding sites in AdcA. Nevertheless, while Zn^{2+} binding is intimately linked to protein conformational changes and uptake of the metal ion, it remains to be determined whether these properties influence interaction between AdcA and AdcB.

In the $AdcA_N$ domain, the metal-binding site is located beneath the surface of the protein and is largely preformed in the absence of ligand. This permits the bioinorganic chemistry of the site to be tightly defined and likely aids in achieving selectivity for Zn^{2+} over other metal ions. This contrasts starkly with cluster A-I SBPs that interact with a broader range of metal ions, such as *S. pneumoniae* PsaA and "*Candidatus* Liberibacter asiaticus" ZnuA2 (32). The metal-binding sites in those SBPs offer greater flexibility in metal-ion coordination. However, this plasticity precludes achieving selectivity and is associated with large-scale protein conformational changes upon ligand binding. Thus, the Zn^{2+}-binding mechanism used by AdcA is a distinct modality from that used by SBPs that recruit other ions. The metal-binding site in the $AdcA_C$ domain is also tightly defined. However, it is highly solvent accessible and is permissive for interaction with Co^{2+} and Ni^{2+} ions, similar to ZinT homologs (33). Despite the interaction of the $AdcA_C$ domain with these ions, the $AdcA_N$ domain is refractory to their binding, and this prevents their import. These insights are also consistent with the observed role of the accessory regions in enhancing Zn^{2+} uptake during growth in limiting conditions. We note that our observations contradict the recent study of Cao et al. (34), who proposed that streptococcal Zn^{2+} import was more readily facilitated by the $AdcA_C$ domain. Our work directly shows that only the $AdcA_N$ domain is necessary and essential for Zn^{2+} import. This discrepancy can likely be attributed to their use of a nonnative gene in their complementation analyses. Our conclusions are also consistent with studies from Gram-negative organisms examining the interaction between ZnuA and ZinT homologs (4, 20, 35). However, it is important to note that a direct interaction between ZinT and other proteins *in vivo* has not yet been observed in Gram-negative species. Our structural and computational data reveal that the $AdcA_N$ domain and the $AdcA_C$ domain form a stable interaction, with the His-rich loop positioned at the interface between the two domains. It is tempting to speculate that the bound Zn^{2+} from the $AdcA_C$ domain is transferred to the $AdcA_N$ domain Zn^{2+} binding site via the dynamic mobility of the His-rich loop. In this way, the $AdcA_C$ domain may enable AdcA to sample Zn^{2+} pools that are spatially inaccessible to the $AdcA_N$ domain and thereby increase the efficiency of its acquisition during severe Zn^{2+} restriction. Collectively, these structural and functional analyses provide crucial insights into how accessory regions and proteins aid metal ion receptors to achieve bacterial Zn^{2+} homeostasis.

In conclusion, our work presents a novel "trap-door" mechanism for Zn^{2+} binding in cluster A-I SBPs. Our findings underscore how the ligand-binding sites of Zn^{2+}-

specific SBPs combine metal specificity with protein-metal interactions. In AdcA, ligand-induced stabilization of highly mobile, local structural elements is crucial for the high-affinity acquisition of Zn^{2+}, a poorly abundant metal ion in host tissues that is essential for pneumococcal colonization and disease. The requirement of *S. pneumoniae* and other pathogens for Zn^{2+} during infection illustrates the therapeutic potential in developing antimicrobials to target crucial, conserved structural elements, such as loop $\alpha 2\beta 2$, and thereby specifically block bacterial Zn^{2+}-uptake pathways *in vivo*.

MATERIALS AND METHODS

Bacterial strains, culturing, and growth experiments. Primers used to generate mutant strains, and plasmids for recombinant protein expression are described in Table S3. Bacterial growth experiments were performed with two technical replicates in at least three independent biological experiments, as described previously (18, 36). Growth curves are presented in Fig. S3. Whole-cell metal accumulation was determined by inductively coupled plasma-mass spectrometry (ICP-MS), using an Agilent 8900 ICP-MS/MS using established methods (36, 37).

Expression, purification, and DSF analysis of AdcA. Mutant variants of recombinant AdcA were generated by site-directed mutagenesis, using primers listed in Table S3A. Wild-type and mutant AdcA variants were expressed in *E. coli* LEMO21(DE3) and purified essentially as described previously (3). Protein samples were analyzed for metal content by heating 5 μM protein at 370 K for 15 min in 3.5% HNO_3, and the metal-ion content was measured by ICP-MS. Differential scanning fluorimetry (DSF) experiments were performed in technical triplicate in at least four independent experiments to determine the mean melting transition (T_m) (36). Fluorescence data (excitation at 470 nm; emission at 570 nm) and the inflection point of the $T_m \pm$ (SEM) were calculated using GraphPad Prism (v7.0d). Affinity determination of the mutant $AdcA_N$ variants was performed essentially as described previously (38).

Protein crystallization, crystal structure determination, and structural analyses. Protein crystals of Zn^{2+}-bound AdcA were obtained in 10% (wt/vol) polyethylene glycol (PEG) 20000, 18% (vol/vol) PEG monomethyl ether (MME) 550, 0.03 M $CaCl_2$, 0.03 M $MgCl_2$, and 0.1 M MES/imidazole (pH 6.5) at 291 K, with a protein concentration of 10 mg ml^{-1} and $ZnCl_2$ at a 1:10 protein/Zn^{2+} molar ratio, using the hanging-drop vapor diffusion method. The $AdcA_N$ domain fragment was crystallized as described previously (39), and the $AdcA_C$ domain fragment was crystallized in 0.1 M sodium acetate (pH 4.5) and 30% (wt/vol) PEG MME 5000 at 293 K. Additional details are provided in Text S1C. Diffraction data collection, processing, and structure refinement statistics can be found in Table S1.

Electron paramagnetic resonance spectroscopy. Labeling of the AdcA-Cys variants (10 μM) was performed by incubation with 100 μM *S*-(1-oxyl-2,2,5,5-tetramethyl-2,5-dihydro-1*H*-pyrrol-3-yl)methyl methanesolfonothionate (MTSSL). Free MTSSL was removed by dialysis (10-kDa MWCO) in 1 liter of buffer solution (20 mM morpholinepropanesulfonic acid [pH 7.2], 100 mM NaCl) at 277 K for 24 h. The dialyzed sample was concentrated to 500 μl (10-kDa MWCO) and purified (Superdex 75 Increase 10/300 column). The sample was concentrated to 100 μM (10-kDa MWCO) and flash-frozen (liquid N_2). X-band CW (continuous wave) EPR spectra in solution were measured on a Bruker Elex E540 spectrometer equipped with a Bruker Super High Sensitivity resonator and a liquid N_2 temperature control system. Instrument parameters are described in Text S1C. Distance distributions were computed from the DEER time traces with DeerAnalysis (40) using the Tikhonov regularization option and a regularization parameter in the range $\lambda = 100$ to 1,000. Tikhonov regularization is a standard mathematical method used to transform the DEER time trace into a model-free distance distribution (i.e., model-free in terms of the shape of the distribution). *In silico* modeling of the spin label rotamer distributions for the metal-free and Zn^{2+}-bound protein conformations was computed using MMM 2018.2 (41).

Molecular dynamics simulations. The crystal structure of Zn^{2+}-bound AdcA was used as the starting structure for all simulations with the set up and parameterization details described in Text S1C. All simulations were carried out using the GROMACS package v5.0.1 (42), in conjunction with the GROMOS 54a7 force field (43) for protein and the simple point charge model for water (44). Analysis was carried out using GROMACS tools. Unless otherwise stated, the five independent simulations for each system were analyzed separately, and only the last 250 ns of each trajectory was used for analysis.

smFRET microscopy and ALEX. The smFRET/ALEX technique was adapted from our prior work (45–47). Stochastic labeling of the Cys-AdcA variant $AdcA_{A73C/A259C}$ used the maleimide derivatives of dyes Alexa-555 and Alexa-647, with further details provided in Text S1C. Labeled $AdcA_{A73C/A259C}$ (25 to 100 pM) was studied with smFRET/ALEX at room temperature (50 mM Tris-HCl [pH 7.4], 1 μM EDTA). All experiments were performed using a bespoke confocal microscope assembly as detailed by Husada et al. (45) and as summarized in Text S1C.

Data availability. The accession codes for the structures deposited in the Protein Data Bank are as follows: 7JJ9 (Zn^{2+}-bound AdcA), 7JJ8 (Zn^{2+}-bound $AdcA_N$), 7JJA (metal-free $AdcA_C$), and 7JJB (Zn^{2+}-bound $AdcA_C$).

SUPPLEMENTAL MATERIAL

Supplemental material is available online only.

TEXT S1, PDF file, 0.2 MB.

TABLE S1, PDF file, 0.1 MB.

TABLE S2, PDF file, 0.1 MB.
TABLE S3, PDF file, 0.1 MB.
FIG S1, PDF file, 2.2 MB.
FIG S2, PDF file, 2.3 MB.
FIG S3, PDF file, 0.9 MB.
FIG S4, PDF file, 0.8 MB.
FIG S5, PDF file, 0.6 MB.
FIG S6, PDF file, 0.7 MB.

REFERENCES

1. Andreini C, Banci L, Bertini I, Rosato A. 2006. Zinc through the three domains of life. J Proteome Res 5:3173–3178. https://doi.org/10.1021/pr0603699.
2. Bayle L, Chimalapati S, Schoehn G, Brown J, Vernet T, Durmort C. 2011. Zinc uptake by *Streptococcus pneumoniae* depends on both AdcA and AdcAII and is essential for normal bacterial morphology and virulence. Mol Microbiol 82:904–916. https://doi.org/10.1111/j.1365-2958.2011.07862.x.
3. Plumptre CD, Eijkelkamp BA, Morey JR, Behr F, Couñago RM, Ogunniyi AD, Kobe B, O'Mara ML, Paton JC, McDevitt CA. 2014. AdcA and AdcAII employ distinct zinc acquisition mechanisms and contribute additively to zinc homeostasis in *Streptococcus pneumoniae*. Mol Microbiol 91:834–851. https://doi.org/10.1111/mmi.12504.
4. Gabbianelli R, Scotti R, Ammendola S, Petrarca P, Nicolini L, Battistoni A. 2011. Role of ZnuABC and ZinT in *Escherichia coli* O157:H7 zinc acquisition and interaction with epithelial cells. BMC Microbiol 11:36. https://doi.org/10.1186/1471-2180-11-36.
5. Pederick VG, Eijkelkamp BA, Begg SL, Ween MP, McAllister LJ, Paton JC, McDevitt CA. 2015. ZnuA and zinc homeostasis in *Pseudomonas aeruginosa*. Sci Rep 5:13139. https://doi.org/10.1038/srep13139.
6. Lhospice S, Gomez NO, Ouerdane L, Brutesco C, Ghssein G, Hajjar C, Liratni A, Wang S, Richaud P, Bleves S, Ball G, Borezee-Durant E, Lobinski R, Pignol D, Arnoux P, Voulhoux R. 2017. *Pseudomonas aeruginosa* zinc uptake in chelating environment is primarily mediated by the metallophore pseudopaline. Sci Rep 7:17132. https://doi.org/10.1038/s41598-017-16765-9.
7. Grim KP, San Francisco B, Radin JN, Brazel EB, Kelliher JL, Parraga Solorzano PK, Kim PC, McDevitt CA, Kehl-Fie TE. 2017. The metallophore staphylopine enables *Staphylococcus aureus* to compete with the host for zinc and overcome nutritional immunity. mBio 8:e01281-17. https://doi.org/10.1128/mBio.01281-17.
8. Ammendola S, Pasquali P, Pistoia C, Petrucci P, Petrarca P, Rotilio G, Battistoni A. 2007. High-affinity Zn^{2+} uptake system ZnuABC is required for bacterial zinc homeostasis in intracellular environments and contributes to the virulence of *Salmonella enterica*. Infect Immun 75:5867–5876. https://doi.org/10.1128/IAI.00559-07.
9. Lewis VG, Ween MP, McDevitt CA. 2012. The role of ATP-binding cassette transporters in bacterial pathogenicity. Protoplasma 249:919–942. https://doi.org/10.1007/s00709-011-0360-8.
10. Karlinsey JE, Maguire ME, Becker LA, Crouch ML, Fang FC. 2010. The phage shock protein PspA facilitates divalent metal transport and is required for virulence of *Salmonella enterica* sv. Typhimurium. Mol Microbiol 78:669–685. https://doi.org/10.1111/j.1365-2958.2010.07357.x.
11. Wang K, Sitsel O, Meloni G, Autzen HE, Andersson M, Klymchuk T, Nielsen AM, Rees DC, Nissen P, Gourdon P. 2014. Structure and mechanism of Zn^{2+}-transporting P-type ATPases. Nature 514:518–522. https://doi.org/10.1038/nature13618.
12. WHO. 2010. Treatment and prevention of pneumonia. World Health Organization, Geneva, Switzerland.
13. Brixner DI. 2005. Improving acute otitis media outcomes through proper antibiotic use and adherence. Am J Manag Care 11:S202–S210.
14. Loisel E, Jacquamet L, Serre L, Bauvois C, Ferrer JL, Vernet T, Di Guilmi AM, Durmort C. 2008. AdcAII, a new pneumococcal Zn-binding protein homologous with ABC transporters: biochemical and structural analysis. J Mol Biol 381:594–606. https://doi.org/10.1016/j.jmb.2008.05.068.
15. Berntsson RP, Smits SH, Schmitt L, Slotboom DJ, Poolman B. 2010. A structural classification of substrate-binding proteins. FEBS Lett 584:2606–2617. https://doi.org/10.1016/j.febslet.2010.04.043.
16. Woo JS, Zeltina A, Goetz BA, Locher KP. 2012. X-ray structure of the *Yersinia pestis* heme transporter HmuUV. Nat Struct Mol Biol 19:1310–1315. https://doi.org/10.1038/nsmb.2417.
17. Korkhov VM, Mireku SA, Hvorup RN, Locher KP. 2012. Asymmetric states of vitamin B_{12} transporter BtuCD are not discriminated by its cognate substrate binding protein BtuF. FEBS Lett 586:972–976. https://doi.org/10.1016/j.febslet.2012.02.042.
18. Couñago RM, Ween MP, Begg SL, Bajaj M, Zuegg J, O'Mara ML, Cooper MA, McEwan AG, Paton JC, Kobe B, McDevitt CA. 2014. Imperfect coordination chemistry facilitates metal ion release in the Psa permease. Nat Chem Biol 10:35–41. https://doi.org/10.1038/nchembio.1382.
19. David G, Blondeau K, Schiltz M, Penel S, Lewit-Bentley A. 2003. YodA from *Escherichia coli* is a metal-binding, lipocalin-like protein. J Biol Chem 278:43728–43735. https://doi.org/10.1074/jbc.M304484200.
20. Ilari A, Alaleona F, Tria G, Petrarca P, Battistoni A, Zamparelli C, Verzili D, Falconi M, Chiancone E. 2014. The *Salmonella enterica* ZinT structure, zinc affinity and interaction with the high-affinity uptake protein ZnuA provide insight into the management of periplasmic zinc. Biochim Biophys Acta 1840:535–544. https://doi.org/10.1016/j.bbagen.2013.10.010.
21. Wei B, Randich AM, Bhattacharyya-Pakrasi M, Pakrasi HB, Smith TJ. 2007. Possible regulatory role for the histidine-rich loop in the zinc transport protein, ZnuA. Biochemistry 46:8734–8743. https://doi.org/10.1021/bi700763w.
22. Banerjee S, Wei B, Bhattacharyya-Pakrasi M, Pakrasi HB, Smith TJ. 2003. Structural determinants of metal specificity in the zinc transport protein ZnuA from *Synechocystis* 6803. J Mol Biol 333:1061–1069. https://doi.org/10.1016/j.jmb.2003.09.008.
23. Lee YH, Dorwart MR, Hazlett KR, Deka RK, Norgard MV, Radolf JD, Hasemann CA. 2002. The crystal structure of Zn(II)-free *Treponema pallidum* TroA, a periplasmic metal-binding protein, reveals a closed conformation. J Bacteriol 184:2300–2304. https://doi.org/10.1128/jb.184.8.2300-2304.2002.
24. Neupane DP, Avalos D, Fullam S, Roychowdhury H, Yukl ET. 2017. Mechanisms of zinc binding to the solute-binding protein AztC and transfer from the metallochaperone AztD. J Biol Chem 292:17496–17505. https://doi.org/10.1074/jbc.M117.804799.
25. Laitaoja M, Valjakka J, Janis J. 2013. Zinc coordination spheres in protein structures. Inorg Chem 52:10983–10991. https://doi.org/10.1021/ic401072d.
26. Yatsunyk LA, Easton JA, Kim LR, Sugarbaker SA, Bennett B, Breece RM, Vorontsov II, Tierney DL, Crowder MW, Rosenzweig AC. 2008. Structure and metal binding properties of ZnuA, a periplasmic zinc transporter from *Escherichia coli*. J Biol Inorg Chem 13:271–288. https://doi.org/10.1007/s00775-007-0320-0.
27. Ilari A, Alaleona F, Petrarca P, Battistoni A, Chiancone E. 2011. The X-ray structure of the zinc transporter ZnuA from *Salmonella enterica* discloses a unique triad of zinc-coordinating histidines. J Mol Biol 409:630–641. https://doi.org/10.1016/j.jmb.2011.04.036.
28. de Boer M, Gouridis G, Vietrov R, Begg SL, Schuurman-Wolters GK, Husada F, Eleftheriadis N, Poolman B, McDevitt CA, Cordes T. 2019. Conformational and dynamic plasticity in substrate-binding proteins underlies selective transport in ABC importers. Elife 8:e44652. https://doi.org/10.7554/eLife.44652.
29. Baker EN, Hubbard RE. 1984. Hydrogen bonding in globular proteins. Prog Biophys Mol Biol 44:97–179. https://doi.org/10.1016/0079-6107(84)90007-5.
30. Abate F, Malito E, Cozzi R, Lo Surdo P, Maione D, Bottomley MJ. 2014. Apo, Zn^{2+}-bound and Mn^{2+}-bound structures reveal ligand-binding properties of SitA from the pathogen *Staphylococcus pseudintermedius*. Biosci Rep 34:e00154. https://doi.org/10.1042/BSR20140088.

31. Pang X, Zhou HX. 2015. Disorder-to-order transition of an active-site loop mediates the allosteric activation of sortase A. Biophys J 109:1706–1715. https://doi.org/10.1016/j.bpj.2015.08.039.
32. Sharma N, Selvakumar P, Bhose S, Ghosh DK, Kumar P, Sharma AK. 2015. Crystal structure of a periplasmic solute binding protein in metal-free, intermediate and metal-bound states from *Candidatus* Liberibacter asiaticus. J Struct Biol 189:184–194. https://doi.org/10.1016/j.jsb.2015.01.012.
33. Kershaw CJ, Brown NL, Hobman JL. 2007. Zinc dependence of *zinT* (*yodA*) mutants and binding of zinc, cadmium, and mercury by ZinT. Biochem Biophys Res Commun 364:66–71. https://doi.org/10.1016/j.bbrc.2007.09.094.
34. Cao K, Li N, Wang H, Cao X, He J, Zhang B, He QY, Zhang G, Sun X. 2018. Two zinc-binding domains in the transporter AdcA from *Streptococcus pyogenes* facilitate high-affinity binding and fast transport of zinc. J Biol Chem 293:6075–6089. https://doi.org/10.1074/jbc.M117.818997.
35. Petrarca P, Ammendola S, Pasquali P, Battistoni A. 2010. The Zur-regulated ZinT protein is an auxiliary component of the high-affinity ZnuABC zinc transporter that facilitates metal recruitment during severe zinc shortage. J Bacteriol 192:1553–1564. https://doi.org/10.1128/JB.01310-09.
36. McDevitt CA, Ogunniyi AD, Valkov E, Lawrence MC, Kobe B, McEwan AG, Paton JC. 2011. A molecular mechanism for bacterial susceptibility to zinc. PLoS Pathog 7:e1002357. https://doi.org/10.1371/journal.ppat.1002357.
37. Begg SL, Eijkelkamp BA, Luo Z, Couñago RM, Morey JR, Maher MJ, Ong CL, McEwan AG, Kobe B, O'Mara ML, Paton JC, McDevitt CA. 2015. Dysregulation of transition metal ion homeostasis is the molecular basis for cadmium toxicity in *Streptococcus pneumoniae*. Nat Commun 6:6418. https://doi.org/10.1038/ncomms7418.
38. Monk IR, Shaikh N, Begg SL, Gajdiss M, Sharkey LKR, Lee JYH, Pidot SJ, Seemann T, Kuiper M, Winnen B, Hvorup R, Collins BM, Bierbaum G, Udagedara SR, Morey JR, Pulyani N, Howden BP, Maher MJ, McDevitt CA, King GF, Stinear TP. 2019. Zinc-binding to the cytoplasmic PAS domain regulates the essential WalK histidine kinase of *Staphylococcus aureus*. Nat Commun 10:3067. https://doi.org/10.1038/s41467-019-10932-4.
39. Luo Z, Morey JR, McDevitt CA, Kobe B. 2015. Heterogeneous nucleation is required for crystallization of the ZnuA domain of pneumococcal AdcA. Acta Crystallogr F Struct Biol Commun 71:1459–1464. https://doi.org/10.1107/S2053230X15021330.
40. Jeschke G, Panek G, Godt A, Bender A, Paulsen H. 2004. Data analysis procedures for pulse ELDOR measurements of broad distance distributions. Appl Magn Reson 26:223–244. https://doi.org/10.1007/BF03166574.
41. Polyhach Y, Bordignon E, Jeschke G. 2011. Rotamer libraries of spin labeled cysteines for protein studies. Phys Chem Chem Phys 13:2356–2366. https://doi.org/10.1039/c0cp01865a.
42. Abraham MJ, Murtola T, Schulz R, Páll S, Smith JC, Hess B, Lindahl E. 2015. GROMACS: High performance molecular simulations through multi-level parallelism from laptops to supercomputers. SoftwareX 1–2:19–25. https://doi.org/10.1016/j.softx.2015.06.001.
43. Schmid N, Eichenberger A, Choutko A, Riniker S, Winger M, Mark A, Gunsteren W. 2011. Definition and testing of the GROMOS force-field versions 54A7 and 54B7. Eur Biophys J 40:843–856. https://doi.org/10.1007/s00249-011-0700-9.
44. Berendsen HJC, Postma JPM, van Gunsteren WF, Hermans J. 1981. Interaction models for water in relation to protein hydration, p 331–342. In Pullman B (ed), Intermolecular forces, vol 14. Springer, Dordrecht, Netherlands.
45. Husada F, Bountra K, Tassis K, de Boer M, Romano M, Rebuffat S, Beis K, Cordes T. 2018. Conformational dynamics of the ABC transporter McjD seen by single-molecule FRET. EMBO J 37:e100056. https://doi.org/10.15252/embj.2018100056.
46. Jazi AA, Ploetz E, Arizki M, Dhandayuthapani B, Waclawska I, Kramer R, Ziegler C, Cordes T. 2017. Caging and photoactivation in single-molecule Forster resonance energy transfer experiments. Biochemistry 56:2031–2041. https://doi.org/10.1021/acs.biochem.6b00916.
47. Gouridis G, Schuurman-Wolters GK, Ploetz E, Husada F, Vietrov R, de Boer M, Cordes T, Poolman B. 2015. Conformational dynamics in substrate-binding domains influences transport in the ABC importer GlnPQ. Nat Struct Mol Biol 22:57–64. https://doi.org/10.1038/nsmb.2929.